How do Velocity Structure Functions Trace Gas Dynamics in Simulated Molecular Clouds?

R.-A. Chira[1], J. C. Ibáñez-Mejía[2,3], M.-M. Mac Low[4,5], and Th. Henning[1]

[1] Max-Planck-Institut für Astronomie, Königstuhl 17, 69117 Heidelberg, Germany
 e-mail: `roxana-adela.chira@alumni.uni-heidelberg.de`
[2] I. Physikalisches Institut, Universität zu Köln, Zülpicher Straße 77, 50937 Köln, Germany
 e-mail: `ibanez@ph1.uni-koeln.de`
[3] Max-Planck-Institut für Extraterrestrische Physik, Giessenbachstrasse 1, 85748 Garching, Germany
[4] Dept. of Astrophysics, American Museum of Natural History, 79th St. at Central Park West, New York, NY 10024, USA
 e-mail: `mordecai@amnh.org`
[5] Zentrum für Astronomie, Institut für Theoretische Astrophysik, Universität Heidelberg, Albert-Ueberle-Str. 2, 69120 Heidelberg, Germany

Preprint online version: June 14, 2018

Abstract

Context. **Supersonic disordered flows accompany the formation and evolution of molecular clouds (MCs). It has been argued that this is turbulence that can support against gravitational collapse and promote the formation of hierarchical substructures. Yet, little is still known about what drives gas dynamics on MC scales.**

Aims. We investigate the time evolution of **gas dynamics** within simulated MCs. We focus on the following questions: What physical process dominantes the driving of **the disordered flows seen? How can these flows be characterized? Are they consistent with turbulence? Do the simulated flows agree with the observations?**

Methods. We follow the gas motions within three MCs that have formed self-consistently within kiloparsec-scale numerical simulations of the interstellar medium (ISM). The simulated ISM evolves under the influence of physical processes including self-gravity, magnetic fields, supernovae-driven turbulence, and radiative heating and cooling. **We characterize the flow using** velocity structure functions n(VSFs) and compare the obtained parameters with predicted **and observed** values.

Results. We demonstrate that the scaling exponent of VSFs and the self-similarity parameter are sensitive tools that trace the dominant driving sources of **the flow**. The trends are generally robust against the influence of projection, Jeans refinement level, and density-weighting. Yet, the detailed evolution may vary significantly depending on the density threshold.

Conclusions. We conclude that the VSF is a well placed and stable method for examining the composition, structure and evolution of turbulence within MCs. Yet, it is essential to clearly define the underlying conditions and assumptions of the analysis in order to clarify which part of the ISM is studied and to make the results comparable to analogue studies. In our case, we find clear indicators of how the VSF reacts to the dynamics in the simulated clouds: Gravitational contraction causes a flattening of the scaling exponent of the structure functions, but has no imprint on the self-similarity parameter of the structure function, unless the collapse is triggered by a shock. Nearby SN explosions inject turbulent energy on a wide range of scales onto MCs. This injection of energy is visible in in the structure functions and the self-similarity parameters, but only for a short period of time as the excess kinetic energy decays. [comparison to observations?]

Key words. keywords

1. Introduction

It has long been known that star formation preferentially occurs within molecular clouds. Yet **the star formation process is still not completely understood**. It is clear that gravity is the major factor as it drives collapse motions and operates on all scales. However, one needs additional processes that stabilise the gas **or terminate star formation quickly** in order to **explain low star formation efficiencies** observed in molecular clouds. Although there are many processes that act at the different scales of molecular clouds, **turbulent support has often been argued** to be the best candidate for this task.

In the literature, turbulence has an ambiguous role in the context of star formation. In most of the cases, turbulence is expected to stabilise molecular clouds on large scales (Fleck 1980; McKee & Zweibel 1992; Mac Low 2003), while feedback processes and shear motions heavily destabilise or even disrupt

cloud-like structures, offering a formation scenario for large filaments (Tan et al. 2013; Miyamoto et al. 2014). [I don't really understand these cites to Tan & Miyamoto. Usually I contrast large scale support with small-scale compressive promotion of collapse.] However, it remains unclear whether there are particular mechanisms that dominate the driving of turbulence within molecular clouds, **as every process is supposed to be traced by typical features in the observables. Yet, these features are either not seen or are too ambiguous to clearly reflect the dominant driving mode.** For example, turbulence that is driven by large-scale velocity dispersions during global collapse (Ballesteros-Paredes et al. 2011a,b; Hartmann et al. 2012) produces P-Cygni lines **that have not yet been observed on scales of entire molecular clouds**. Internal feedback, on the contrary, seems more promising as it drives turbulence outwards (Dekel & Krumholz 2013; Krumholz et al. 2014). Observations, though, demonstrate that the required driving sources need to act

on scales of entire clouds; which typical feedback, **such as radiation, winds, jets, or supernovae (SNe),** cannot achieve (Heyer & Brunt 2004; Brunt et al. 2009; Brunt & Heyer 2013).

There have been many theoretical studies that have examined the nature and origin of turbulence within the phases of the interstellar medium (ISM; Mac Low & Klessen 2004, and references within). The most established **characterization of turbulence in general was** by Kolmogorov (1941) who investigated fully developed, incompressible turbulence **driven on scales larger than the object of interest, and diffusing on scales much smaller than those of interest**. In the scope of this paper this object is a single molecular cloud. Molecular clouds are highly compressible, though. Only a few analytical studies have treated this case. She & Lévêque (1994) and Boldyrev (2002), for example, generalise and extend the predicted scaling of the decay of turbulence to supersonic turbulence. Galtier & Banerjee (2011) and Banerjee & Galtier (2013) provide an analytic description of the scaling of mass-weighted structure functions.

In this paper, we examine three molecular clouds that formed **self-consistently** from SN-driven turbulence in the simulations by Ibáñez-Mejía et al. (2016, 2017, Paper I and Paper II hereafter) and study how the turbulence within the clouds' gas evolves. The key questions we **address** are the following: What dominates the turbulence within the simulated molecular clouds? **How can structure functions inform us about the evolutionary state of MCs and the dominant physics processes within them?**

In Sect. 2, we introduce the simulated clouds in the context of the underlying physics involved in the simulations. Furthermore, we describe the theoretical basics of velocity structure functions. Sect. 3 demonstrates that the velocity structure function is a useful tool to characterise the dominant driving mechanisms of turbulence in molecular clouds and can be applied to both simulated and observed data. We also discuss the influences of utilising one-dimensional velocity measurements, different Jeans refinement levels, density thresholds and density weighting on the applicability of the velocity structure function and the results obtained with it in Sect. 4. We summarise our findings and conclusions in Sect. 5.

2. Methods

2.1. Cloud models

The analysis in this paper is based on a sample of three molecular clouds (MCs) found within a **three-dimensional, magnetohydrodynamical, adaptive mesh refinement simulation by Paper I, using the FLASH code (Fryxell et al. 2000). Paper I; Paper II, as well as Chira et al. (2018, Paper III hereafter)** describe the simulations and the clouds in more detail. We summarise the most relevant properties.

The numerical simulation models a $1 \times 1 \times 40$ **kpc**^{3} section of the multi-phase, turbulent ISM of a disk galaxy, where dense structures form self-consistently in convergent, turbulent flows (Paper I). The model includes gravity—a background galactic-disk potential accounting for a stellar component and a dark matter halo, as well as self-gravity turned on after 250 Myr of simulated time—SN-driven turbulence, photoelectric heating and radiative cooling, and magnetic fields. Although hundreds of dense clouds form within the simulated volume, Paper II focused on three clouds, which were re-simulated at a much higher spatial resolution, **which we map to a uniform grid of 0.1 pc zones.** In this paper, we use the data within (40 pc)^3 subregions centred in the high-resolution clouds' centres of mass. The inter-

nal structures of MCs are resolved using adaptive mesh refinement, focusing grid resolution on dense regions where Jeans unstable structures must be resolved with a minimum of 4 cells ($\lambda_J > 4 \, \Delta x_{\min}$). For a maximum resolution of $\Delta x = 0.1$ pc, the corresponding maximum resolved density is 8×10^3 cm^{-3} for gas at a temperature of 10 K (e.g. Paper II, Eq. 15). This means that we can trace fragmentation down to 0.4 pc, but cannot fully resolve objects that form at smaller scales. The MCs have initial masses at the onset of self-gravity of 3×10^3, 4×10^3, and 8×10^3 M$_\odot$ and are denoted as M3, M4, and M8, respectively, hereafter.

However, it is important to point out that the clouds are embedded within a complex turbulent environment, gaining and losing mass as they evolve. **Paper II described the time evolution of the properties of all three clouds in detail, in particular, mass, size, velocity dispersion, and accretion rates, in the context of MC formation and evolution within a galactic environment.** Paper III studied the properties, evolution, and fragmentation of filaments that self-consistently condense within these clouds. They paid particular attention to the accuracy of typical stability criteria for filaments, comparing their measurements to the theoretical predictions, showing that theoretical models do not capture the complexity of fragmentation due to their simplifying assumptions.

In this paper, we focus on the driving sources of turbulence within the simulated MCs and the signatures they imprint on **the velocity structure function (VSF)**.

2.2. Velocity Structure Function

We probe the power distribution of turbulence throughout the entire simulated MCs by using the VSF. The VSF is a two-point correlation function,

Definition 1. $S_p(\ell) = |\Delta v(\ell)|^p$,

that measures the mean velocity difference, $\Delta v(\ell) = v(x + \ell) - v(x)$, between two points x and $x + \ell$ (with ℓ being the direction vector pointing from the first to the second point), to the pth power as function of lag distance, $\ell = |\ell|$, between the correlated points. The VSF estimates the occurrence of symmetric motions (e.g., rotation, collapse, outflows), as well as rare events in random turbulent flows (e.g., SNe) in velocity patterns. Those patterns become more prominent the higher the order p is (Heyer & Brunt 2004).

Padoan et al. (2016) defined a density-weighted structure function

Definition 2. $S_p(\ell) = \frac{\langle \rho(x)\rho(x+\ell) |\Delta v|^p \rangle}{\langle \rho(x)\rho(x+\ell) \rangle}$.

The first several orders of the VSF have a physical meaning. For example, S_1 **gives the mean of relative velocities between any two points** reflecting the modes created by different gas flows, while S_2 is proportional to the kinetic energy, making it a good probe of how the turbulent energy is **distributed among** different scales.

For fully developed turbulence the VSF is well-described by a power-law relation (Kolmogorov 1941; She & Lévêque 1994; Boldyrev 2002):

$$S_p(\ell) \propto \ell^{\zeta(p)}. \tag{1}$$

Note that the scaling exponent of that power-law relation, ζ, depends on many parameters, such as the order of the VSF, as well as the properties and composition of the studied turbulent flow,

such as its geometry, compressibility, or magnetization. Many studies of VSFs distinguish between longitudinal and transverse velocity components, or compressible and solenoidal components, because those are expected to behave differently, especially towards larger lag distances (Gotoh et al. 2002; Schmidt et al. 2008; Benzi et al. 2010). However, the differences are mostly negligible on the scales we focus on. **Since these decompositions are also hard to perform on observational data, we focus only on the total VSF.**

Theoretical studies predict values of ζ depending on the nature of the turbulence and the order p. For example, Kolmogorov (1941) predicts that the third-order exponent, $\zeta(3)$, is equal to unity for an **incompressible flow**. This results in the commonly known prediction that the kinetic energy decays with $E_{\mathrm{kin}}(k) \propto k^{-\frac{5}{3}}$, with $k = \frac{2\pi}{\ell}$ being the wavenumber of the turbulence mode.

For a supersonic flow, however, $\zeta(3) > 1$ **is expected.** Based on Kolmogorov's work, She & Lévêque (1994) and Boldyrev (2002) extended and generalised the analysis and predicted the following. For an incompressible filamentary flow She & Lévêque (1994) predict that the VSFs scale with,

$$\zeta(p) = \frac{p}{9} + 2\left[1 - \left(\frac{2}{3}\right)^{\frac{p}{3}}\right], \tag{2}$$

while supersonic flows with sheet-like geometry are supposed to scale with (Boldyrev 2002),

$$\zeta(p) = \frac{p}{9} + 1 - \left(\frac{1}{3}\right)^{\frac{p}{3}}. \tag{3}$$

Benzi et al. (1993) introduced the principle of extended self-similarity. It proposes that there is a constant relationship between the scaling exponents of different orders at all lag scales. **The self-similarity parameter is defined as,**

Definition 3. $Z(p) = \frac{\zeta(p)}{\zeta(3)}$.

Since **the predicted values for $\zeta(p)$ by She & Lévêque (1994) and Boldyrev (2002)** are normalised so that $\zeta(3) = 1$, Eq. (2) and (3) also provide the predictions for $Z(p)$, respectively.

For the discussion below, we measure ζ by fitting a power-law, given by

$$\log_{10}\left[S_p(\ell)\right] = \log_{10}(A) + \zeta \log_{10}(\ell), \tag{4}$$

with A being the proportionality factor of the power-law to the simulated measurements. For the calculations, we only take cells with a minimal number density of 100 cm^{-3} into account as this threshold defines the volume of the clouds. **In order to reduce** the computational effort, we divide the range of three-dimensional lag distances, $|\boldsymbol{\ell}|$, into 40 equidistantly separated bins ranging from 0.1 to 30 pc. **[there must be more to your optimization method than this. Fill in the details?]** This means that the measurements at the given lag interval ℓ_i we will show below are based on data with lag distances $\ell_{i-1} < \ell \le \ell_i$.

3. Results

In this section, we present our results on how velocity structure functions (VSFs) reflect the distribution of turbulent power within molecular clouds.

3.1. Examples

Fig. 1 shows three examples of VSFs, (a) cloud M4 at $t = 1.2$ Myr after self-gravity has been activated in the simulations, (b) M3 at $t = 3.5$ Myr, and (c) M3 at $t = 4.0$ Myr. All plots show the **density-weighted** VSFs of orders $p = 1$–3. The solid lines show the fitted power-law relations as given in Eq. (4).

The examples demonstrate that, in general, the measured VSFs cannot be described by a single power-law relation over the entire range of ℓ. Instead they are composed of roughly three different regimes: one at small scales at $\ell \lesssim 3$ pc, a second one within 3 pc $\lesssim \ell \lesssim$ 10–15 pc, and the last one at large scales with $\ell > 15$ pc. **We find that** only the small and intermediate ranges may be represented by a common power-law relation. On larger scales, one observes a local minimum before the VSFs either increase or stagnate. The location of the minimum coincides with the equivalent radius of the cloud, the radius a cloud of given mass would have if it would be a sphere. **[this is a pretty big claim to make based on one example. Can you make a plot showing the minimum location vs the equivalent radius for all three clouds for several times? Otherwise, I'd consider cutting it.]** Thus, in this context the VSF is an accurate tool to measure the size of a molecular cloud. On smaller scales, which correspond to individual clumps and cores, one sees significant differences.

The examples in Fig. 1 illustrate how VSFs react to different scenarios that affect the turbulent structure of the entire clouds. **Fig. 1(a) shows the case where turbulence is driven on large scales and naturally decays towards smaller scales. This is the most common behavior seen in all three MCs within the first ~1.5 Myr of the simulations.** During this interval of time the clouds experience the effect of self-gravity for the first time in their evolution and need to adjust to this new condition. Until this is the case, their VSFs are dominated by the freely cascading turbulence that previously dominated the kinetic structure of the clouds. Furthermore, this implies that we can only reliably examine turbulence within the simulations after 1.5 Myr and carefully need to take this into account in the further discussion (see Ibáñez-Mejía et al. 2017; Seifried et al. 2017).

The other examples represent the clouds at later stages of their evolution when the VSFs are dominated by sources that drive the **low** within the clouds in a more extreme way. Fig. 1(b) shows the VSF of M3 at a time when the cloud has just been hit by a SN shock front. One clearly sees how the amplitude of the VSFs is increased by one to two orders of magnitudes compared to the previous example. Especially the power **at small scales ($\ell \lesssim$ few parsecs) is highly amplified as a result of the shock, while it also reduces** the equivalent radius of the cloud. **[is that first minimum the thickness of the post-shock region, or the equivalent radius of the cloud? I'd bet that it's the former.]** Despite the increase of turbulent power at small scales, a large amount of energy is injected at large scales, as well. All this results in a **shallower slope of the VSF**. However, the effect of SN shocks last for only a short period of time (see below).

The last example, Fig. 1(c), demonstrates the imprint of gravitational contraction. Here, the VSF is almost flat, or even slightly increasing towards smaller separation scales. This kind of profile is typical for gas that is self-gravitationally contracting (Boneberg et al. 2015; Burkhart et al. 2015) since gas moves into the inner regions of the cloud, reducing the average lag distances, but not necessarily the relative velocities. The latter may even be accelerated by the infall. As a consequence, large amounts of kinetic energy are transferred to smaller scales which flattens the corresponding VSF.
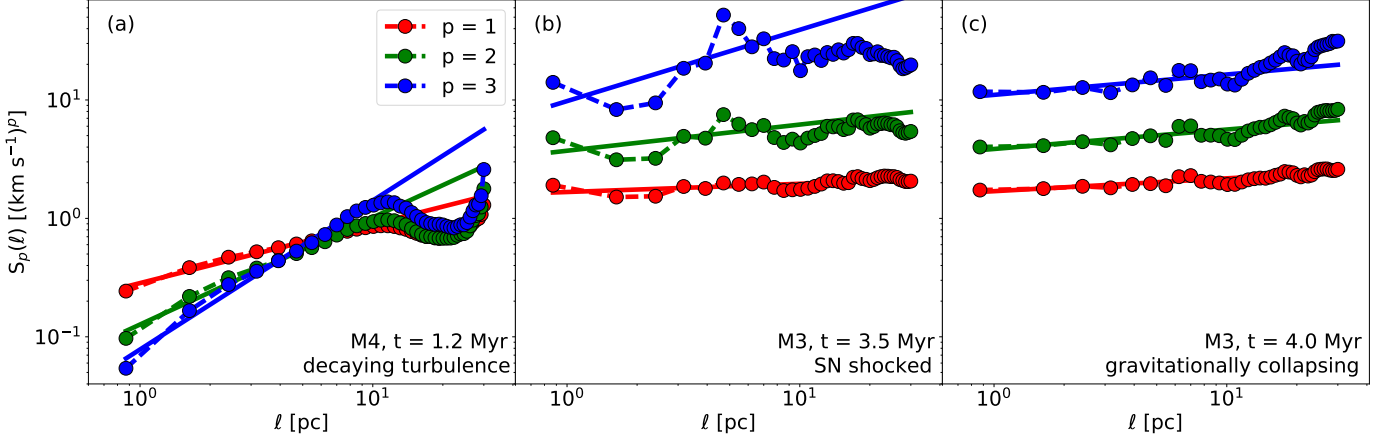
Figure 1: Examples of velocity structure functions as function of the lag scale, ℓ, and order, p. The dots (connected by dashed lines) show the values computed from the simulation. The solid lines represent the power-law relations fitted to the respective structure functions.

3.2. Time Evolution

Fig. 2a plots the time evolution of ζ obtained for all three clouds. The figure shows several interesting features. First, initially, at $t = 0$ Myr, all calculated values of ζ are above the predicted values (see Eqs. (2) and (3)). This means that the turbulence within the clouds is highly supersonic before the gas begins to react to the activation of self-gravity. Second, all ζ decrease with time as the clouds gravitationally collapse. **This gravitational collapse causes gas around the collapsing centers to accelerate, increasing the relative velocities at small scales. This process leads to the flattening of the exponent of the structure function, ζ, as a function of time.** Third, occasionally one observes bumps and dips in all orders of VSFs (e.g., M3 or M8 around $t = 1.7$ Myr). These features only last for short periods of time (up to 0.6 Myr), but set in quasi-instantly and represent a complete relocation of the turbulent power particularly on large scales.

M8 seems to develop differently. At the time the SN occurring at $t = 0.8$ Myr hits the cloud the values of ζ do not rise, as they have done within the other two clouds, but instead they drop. After the shock all scaling exponents grow to levels that are slightly above the pre-shock values, before they slowly decrease again.

Fig. 3a shows the time evolution of the self-similarity parameter, Z, based on the model clouds. One sees that most of the time the measured values of Z are in agreement or at least closely approaching the predicted values. The peaks in the Z (for example, in M4 at $t = 4.1$ Myr) occur at the times when the scaling exponents of the VSFs, ζ, reach values close or below 0. The decrease in Z (for example, in M3 around $t = 1.8$ Myr), on the other hand, occur when SN shocks hit and heavily impact the clouds.

In the following of this section, we will present how VSFs react to variety of setups that are typically assumed in comparable studies. We will compare the findings with the results we have obtained with our original setup. In Sect. 4, we will discuss and interpret these results in more details.

3.3. Comparison to Line-of-Sight Velocities

Previously, we have seen how the VSF behaves and evolves within the clouds. By doing so, we derived the relative velocities based on the 3D velocity vectors that we read out from the simulations. Yet, this method is rather not applicable for many other studies. It is either computational expensive or not possible as observations generally only provide the velocity component along the line-of-sight (los). Thus, in this subsection we investigate how VSFs derived from 1D relative velocities compare to the 3D VSFs presented before. Thereby, we define the 1D VSF as follows:

$$S_p^{1D}(\ell) = \frac{\langle \rho(\boldsymbol{x})\rho(\boldsymbol{x} + \boldsymbol{\ell}) \, |\Delta \boldsymbol{v} \cdot \boldsymbol{e}_i|^p \rangle}{\langle \rho(\boldsymbol{x})\rho(\boldsymbol{x} + \boldsymbol{\ell}) \rangle}, \qquad (5)$$

with $\boldsymbol{e}_i$ representing the unit vector along the $i = $ x-, y-, or z-axis. Figs. 2b and 3b show measured ζ and Z, respectively, derived based on Eq. (5). We see that, in most of the cases, all 1D VSFs agree well with each other, as well as with the corresponding 3D VSFs. Yet, there are cases in which the 1D VSF evolves temporarily or completely differently than the 3D VSF. For example, the 1D VSF along the x-axis in M3 initially behaves like the corresponding 3D VSF, if though with lower absolute values of ζ (or higher values of Z). However, within $t = 2.5$–3.8 Myr the samples diverge. While the 3D based ζ cease further and switch signs, the ζ based on the 1D VSF along the x-axis show a local maximum before converging with the 3D ζ again.

3.4. The Effect of Density Thresholds

Another assumption that significantly influence the structure and evolution of VSFs is the (number) density threshold, n_{cloud}, that is normally applied to filter out the cells that are part of the clouds. In this paper, we assume a minimal number density of $n_{\text{cloud}} = 100$ cm^{-3}. This means that, when focusing on the cloud-only gas, we only consider those cells with number densities $n \geq n_{\text{cloud}}$. We have chosen this threshold as it roughly corresponds to the density when CO becomes detectable.

However, Paper II show that there is usually no harsh increase in density between the ISM and the clouds. Instead, the gas becomes continuously denser towards the centres of mass within the clouds. Consequently, introducing a density threshold is a rather artificial, physically weakly motivated distinction between the clouds and the ISM. Observationally, however, introducing a density (or intensity) threshold is unavoidable, be it due to technical limitations (e.g., sensibility of detector) or the nature of the underlying physical processes (for example, excitation rates, or critical density). Therefore, it is important to study
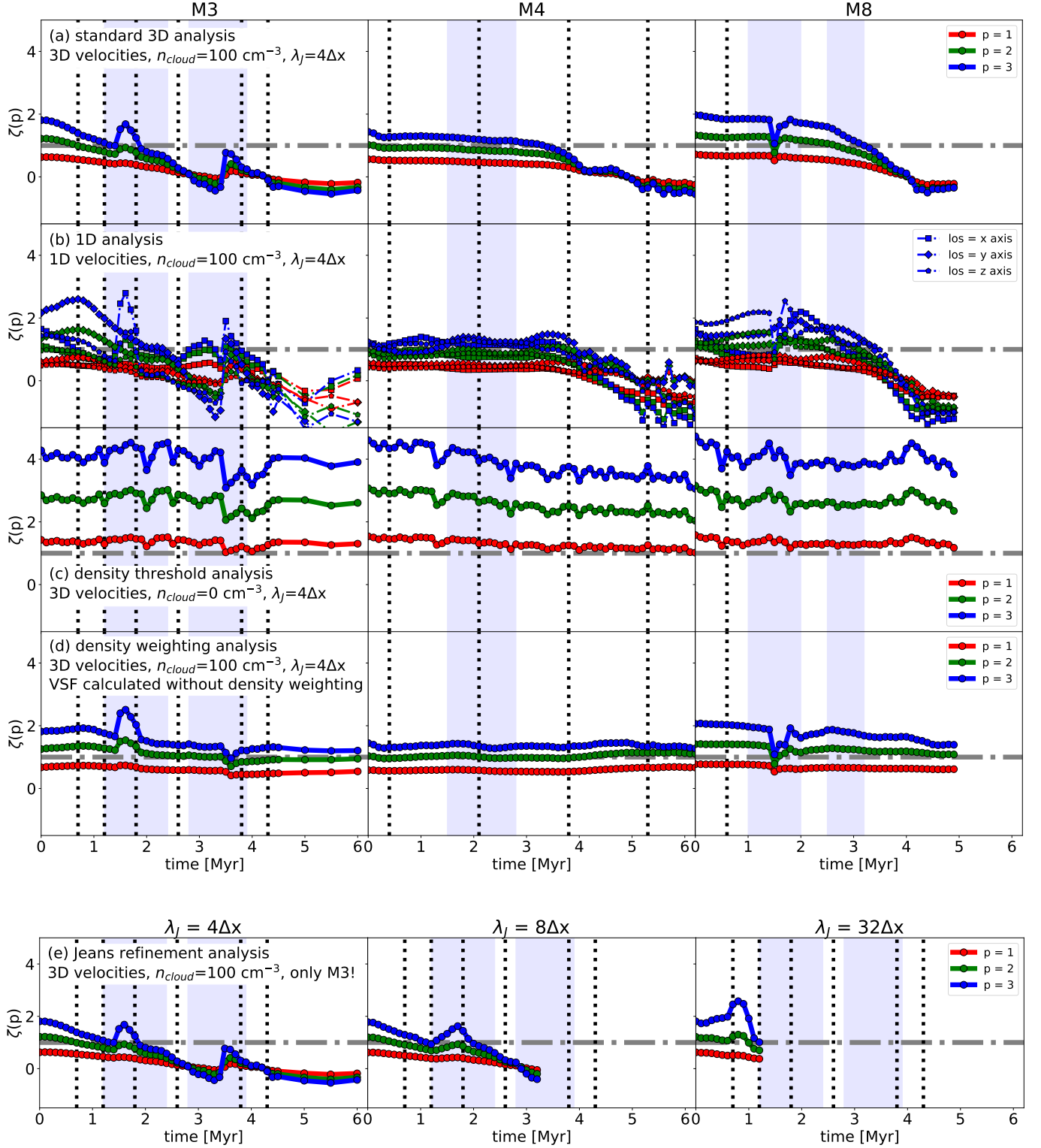
Figure 2: Time evolution of scaling exponent ζ of the pth order VSF. The plots (a) − (d) show the measurements for M3 (*left*), M4 (*middle*), and M8 (*right*), respectively. Thereby, (a) represents the standard analysis while the other rows illustrate the results of the test scenarios with input parameters adjusted as mentioned in the fiugures. The plots of (e) show the values of ζ measured within M3 as function of the respective Jeans refinement level the cloud has been modelled with. The grey dotted vertical lines point to the times than a SN explodes within the vicinity of the corresponding cloud, while the blue areas indicate the time of enhanced mass accretion onto the clouds.
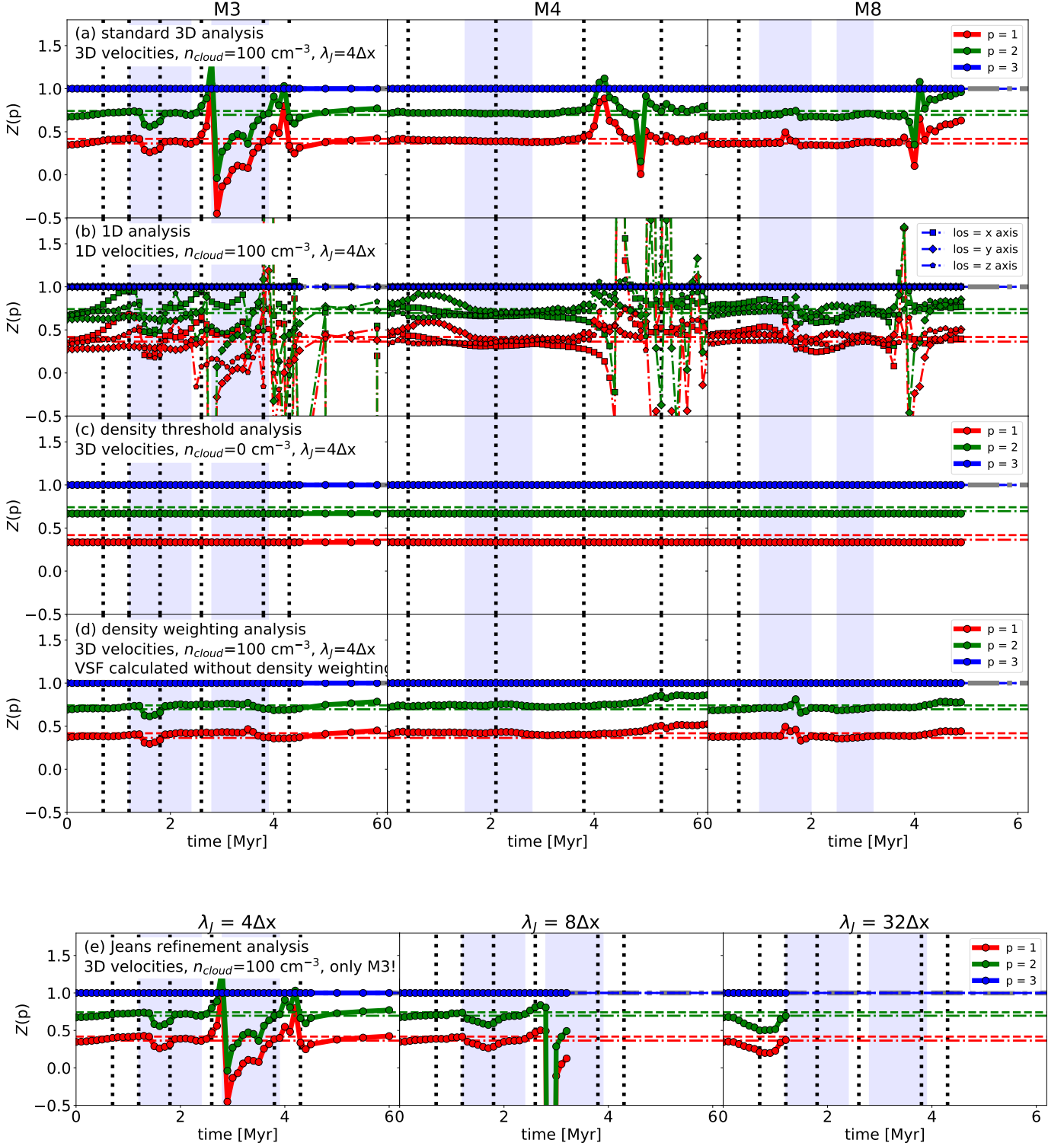
Figure 3: Like Fig. 2, but for the measured self-similarity parameter $Z = \zeta(p)/\zeta(3)$ of the pth order VSF. The coloured horizontal lines show the predicted values by She & Lévêque (1994) (dash-dotted lines) and Boldyrev (2002) (dashed lines).

to which extend a density threshold influences the VSF and its evolution.

Furthermore, this approach considers only ≤1.5% of the cubes' volumes. Removing the density threshold, by setting $n_{\text{cloud}} = 0$ cm^{-3}, would results in analysing the data of the entire data cubes. **As this would be too computational expensive for the test scenario we present here, we randomly choose a set of 5% of the total number of cells as reference points and compute relative velocities to these cells only. We emphasise that this does not mean that we only calculate the**

relative velocities between those 5% of cells. Rather this sub-sample of cells represent the starting vectors x to which the velocities of all other cells $x+\ell$ in the same cube are compared to. This way we reduce the risk of ignoring or emphasising any spatial direction or angle.**

Note that by choosing the starting points randomly we ensure that all parts of the cubes are considered. As a consequence, there is only a little likelihood ($5\% \times 1.5\% = 0.075\%$) that cells that are associated with the clouds are chosen. Therefore, we emphasise that it is likely that the two subsamples (no density threshold and cloud-only) do not necessarily have a common subset of starting vectors. Yet, as we here still calculate relative velocities to all other cells in the cube, and that includes all cells making up the clouds, the resulting VSFs of the $n_{cloud} = 0$ cm^{-3} sample also consists of most of the information of the inner-cloud interactions.

In Figs. 2c and 3c we show the measured values of ζ and Z, respectively, that are derived from the data cubes without introducing an density threshold, meaning $n_{cloud} = 0$ cm^{-3}. This means that we now do not only calculate the relative velocities between cells that are part of the clouds' volume, but between cells within the entire 400^3 cell cut-outs that contain both the clouds and the ISM. For our calculations we apply the same methods as described in Sect. 2. Yet, in order to reduce the computational effort we choose only a randomly positioned subset of 3,200,000 cells (= 5% of the entire 400^3 cube) within the entire cubes as reference points, x. As the clouds make up only a small fraction of the volume within the cubes ($\approx 1.5\%$), this approach makes it more like to pick locations within the modelled ISM, rather than cells within the clouds. We emphasise that, by doing so, we only influence the choice of x in Eq. (1), not $x + \ell$ as we still compute the relative velocities relative to every other cell at 3D lag distance ℓ within the entire cube.

Figs. 2c and 3c clearly illustrate that the measurements in the samples without density threshold completely differ from those with the density threshold. Fig. 2c shows that the measured values of ζ are by far higher in the ISM than in the cloud-only sample. Although we see a similar decline of ζ in M4 and M8 as the gas contracts under the influence of gravity in the vicinity of the clouds, ζ generally evolve differently here than what we have observed for the cloud-only matter. E.g., the pronounced features that have reflected the interactions between the clouds' gas and shock waves are either not as significantly visible or not present at all. We see a high rate of random fluctuations in the evolution of ζ, as well. Furthermore, contrary to all of our other test scenarios, we see here that all Z are constant in time and within all clouds, with values slightly lower than those predicted by She & Lévêque (1994) for filamentary flows.

3.5. The Effect of Density Weighting

As mentioned in Sect. 2.2, Eq. (1) represents the definition of the density-weighted VSF. The density weighting is required for this study to account for obtaining the data from smooth density distributions on Eulerian grids, instead of using individual Lagrangian test particles (or eddies) as it is actually supposed to. Thus, the question is: How the two approaches compare with each other? There are a few studies that have targeted this question (e.g., Benzi et al. 1993, 2010; Gotoh et al. 2002; Schmidt et al. 2008). However, all of them considered turbulent flows in sterile, homogeneous environments that are not comparable to our clouds. Other studies, like Padoan et al. (2016), use both methods, but not on the same set of data.

In this section, we investigate the influence of density weighting on VSFs by repeating the original analysis with the non-weighted VSF given by,

$$S_p(\ell) = \langle |\Delta v|^p \rangle = \langle |v(x) - v(x + \ell)|^p \rangle. \tag{6}$$

Figs. 2d and 3d show the measured values of ζ and Z derived from the non-weighted VSFs, respectively.

Comparing the weighted and non-weighted samples, we see the following: The non-weighted ζ (Fig. 2d) and Z (Fig. 3d) trace the interactions between the gas of the clouds and the SN shocks in the same way as we have seen it for the density-weighted VSF. In M3 and M8 we also see that the values of ζ decrease as the clouds evolve, yet not as fast as they do in the density-weighted VSFs. The measurements in M4, however, are almost constant over time. In all the cases, the values of ζ never cease below 0.5; a behaviour that clearly differs from what we have observed in the density-weighted VSFs.

We observe a similar behaviour for measured Z. As before, they are almost constant over time and in good agreement with predicted values. The only derivations we see compared to the previous results are caused by the interactions between the clouds and incoming SN shock fronts, with levels of disturbance that are similar to the measurements using density-weighted VSFs. However, the evolution of Zs is smoother as there is no sign inversion of ζ. This means that we do not have any strong peaks in Z indicating the time when $\zeta(3)$ approaches 0, which happened when the majority of the turbulent power has been transferred to the small scales.

Fig. 4 summarises the comparison of ζ (*top*) and Z (*bottom*) measured with the density-weighted (*abscissas*) and non-weighted VSFs (*ordinates*) for all Jeans refinement levels **(meaning the granularity used for modelling the turbulent motions of the gas, see Sect. 3.6 for more details)**. The figure clearly shows that the measurements only agree well for the highest refinement level with $\lambda = 32\Delta x$. However, we would need more data point to be sure that this correlation is indeed real. At lower refinement level the measurements, **as those used for the standard analysis and all other test scenarios but the one presented in Sect. 3.6,** correlate less well with each other. The differences in the samples appear dominantly when the density-weighted ζ cease below ≈ 0.5, which is the global minimum for the non-weighted ζ. This means that none of the ζ computed in all clouds and refinement levels with the non-weighted VSF is measured to be below 0.5.

3.6. The Effect of Jeans Length Refinement

The results we have discussed so far are based on simulation data as they have been presented in Paper I and Paper II. Due to the huge computational expense the variety of physical and numerical processes (fluid dynamics, adaptive mesh refinement, supernovae, magnetic fields, radiative heating and cooling, and many more) within those simulations, though, have demanded some compromises.

One of these compromises has been the Jeans refinement criterion as part of the AMR mechanisms. The authors have resolved local Jeans lengths by only four cells ($\lambda_J = 4\Delta x$). This is the minimal requirement for modelling self-gravitating gas in order to avoid artificial fragmentation (Truelove et al. 1998). Other studies, for example by Turk et al. (2012), have shown that a significant higher refinement is needed to reliably resolve turbulent structures and flows on scales of individual cells.

In the appendix of Paper II, the authors examine the effect the number of cells used for the Jeans refinement has on the mea-
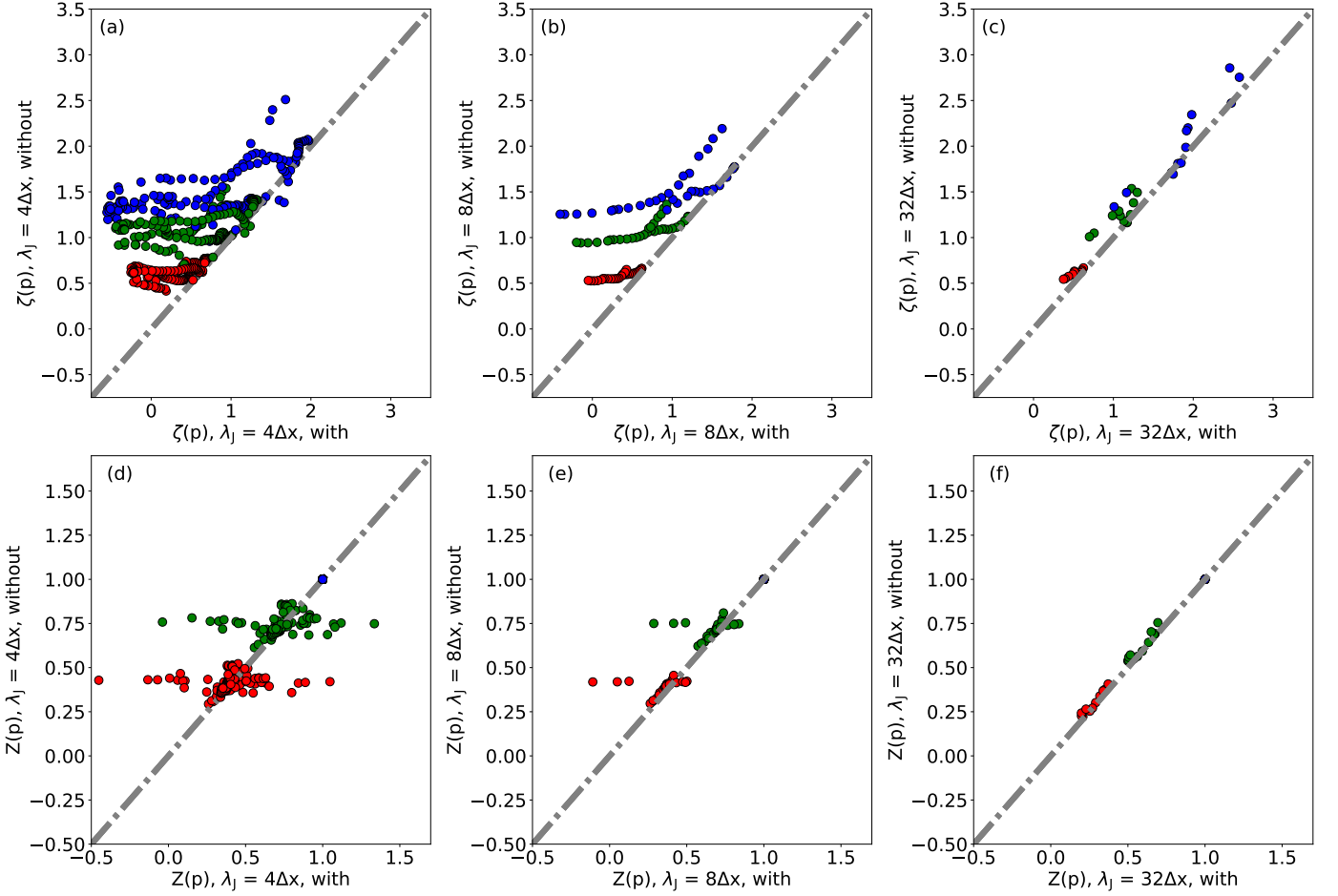
Figure 4: Comparison of ζ (*top*) and Z (*bottom*) measured based on density-weighted VSFs (*abscissas*) and non-weighted VSFs (*ordinates*).

sured kinetic energy. For this, they have rerun the simulations of M3 twice; once with a refinement of eight cells per Jeans length ($\lambda_J = 8\Delta x$) for the first 3 Myr after self-gravity was activated, and once with 32 cells per Jeans length ($\lambda_J = 32\Delta x$) for the first megayear of the cloud's evolution. The authors show that the $\lambda_J = 32\Delta x$ simulations smoothly reveal the energy power spectrum on all scales already after this first megayear. The other two setups do this, as well. However, they need more time to overcome the resonances in the respective power spectra that originate from the previous resolution steps. This is why one can only then fully reliably trust the findings in this paper after the clouds have evolved for approximately 1.5 Myr (see also Ibáñez-Mejía et al. 2017; Seifried et al. 2017).

Furthermore, Paper II have calculated the difference in the cloud's total kinetic energy as function of time and refinement level. They found that the $\lambda_J = 4\Delta x$ simulations miss a significant amount of kinetic energy, namely up to 13% compared to $\lambda_J = 8\Delta x$ and 33% compared to $\lambda_J = 32\Delta x$. However, they also observed that these differences peak around $t = 0.5$ Myr and decrease afterwards, as the $\lambda_J = 4\Delta x$ and $\lambda_J = 8\Delta x$ simulations adjust to the new refinement levels. This, of course, means that the results we have derived from the $\lambda_J = 4\Delta x$ simulations always needs to be evaluated with respect to this lack of energy, although the clouds' dynamics is dominated by gravitational collapse. It also means that the $\lambda_J = 4\Delta x$ data become more reliable the longer the simulations have time to evolve.

In this section, we present how the level of Jeans refinement influences the behaviour of the VSFs. In order to do so, we investigate the M3 data of the $\lambda_J = 8\Delta x$ and $\lambda_J = 32\Delta x$ simulations in the same way as we have done with the $\lambda_J = 4\Delta x$ data: measure the VSFs and analyse the time evolution of ζ and Z. Figs. 2e and 3e show the measure values of ζ and Z for the $\lambda_J = 8\Delta x$ and $\lambda_J = 32\Delta x$. In Fig. 5 we directly compare the measurements of all refinement levels relative to $\lambda_J = 4\Delta x$.

$\lambda_J = 8\Delta x$ shows the same behaviour as $\lambda_J = 4\Delta x$ previously, with values in both samples being in good agreement as the top panel of Fig. 5 demonstrates. Over the entire observed time span, the measured values of ζ decreases as the VSF become flatter. At the time the SNe interact with the cloud, the VSFs steeply increase forward larger scales, causing values of ζ (Fig. 2e). Compared to the $\lambda_J = 4\Delta x$ sample, the peak in ζ is smoother and last longer here, reflecting an impact time span of a bit less than 1 Myr.

This is observable in Fig. 3e where the sink of Z due to the SN shock lasts longer than it has done in within the $\lambda_J = 4\Delta x$ simulations. Besides this, the time evolution of Z based on the $\lambda_J = 8\Delta x$ simulations is as sensitive to the turbulence-related events as it has been for $\lambda_J = 4\Delta x$. The divergence which is produced when gravity has transferred the majority of power to smaller scales occurs at the same time. Thereby, the depth of the sink is a numerical artefact caused by $\zeta(3)$ being equal or close to 0 at this very time step.

The picture changes when we analyse the VSFs based on the $\lambda_J = 32\Delta x$ runs (Figs. 2e, 3e, and 5). Here one sees that the measured values of both ζ (Fig. 2e) and Z (Fig. 3e) are similar to those for $\lambda_J = 4\Delta x$ for the first 0.2 Myr. After this short period, though, the evolutions of ζ diverge. While $\zeta(1)$ and $\zeta(2)$ continue to decrease in similar, but on lower rates compared to $\lambda_J = 4\Delta x$, $\zeta(3)$ increases until it peaks at $t = 0.8$ Myr and falls steeply down again. This divergence has notable impact on the evolution of Z, as well. The bottom panel of Fig. 5 illustrates the different evolutions of measured ζ and Z in the two samples of simulations more clearly. One sees that the differences between the samples follow the same pattern for all orders of p. The differences, though, increases with the order: While the values for $\zeta(1)$ are still in good agreement, the measured values of $\zeta(2)$ and $\zeta(3)$ for $\lambda_J = 32\Delta x$ are 40% and 100% higher than those measured for $\lambda_J = 4\Delta x$, respectively. Consequently, this causes differences in $Z(p)$ within 30–52% between the simulations.

At $t = 1.2$ Myr, the last time step of this sample, the values of all ζ equal the measurements of $\lambda_J = 4\Delta x$ again. As there is no information of how the $\lambda_J = 32\Delta x$ simulations develop further we cannot predict whether this correspondence will continue.

4. Discussion

4.1. Time Evolution

In Sect. **??** we have seen that the shape of VSFs measured for the gas of simulated molecular clouds evolves in the same way as the clouds themselves. For example, Fig. 2a demonstrates that the measured ζ cease with time as the clouds contract under the influence of self-gravity. This is evident as the density and boundness of the clouds increases **as** further gas falls into them (Paper II).

However, one also sees peaks in the profiles of ζ that represent a temporary deviation from the global evolution of the clouds. The origin of these features can easily be traced back to the SNe occurring in the environment of the clouds. To visualise this better, we add marks to Fig. 2 that represent the times when the SNe explode and the periods of time when the clouds are heavily accreting gas. The data are taken from Paper II, where mean distances between the sites of SNe and the centres of the clouds can also be found. Considering that the SNe shock fronts move at speeds of 50–100 km s^{-1} through the ISM and with distances between 30–100 pc to the clouds, the shocks need around 1 Myr, on average, to reach the clouds. Thus, one cannot only relate the major gas accretion events of the clouds to the arrival of those SNe, that indeed affect the evolution of the clouds, but also all significant variations in the evolution of ζ. In most of the cases, the SNe inject turbulent power into the systems. This amplifies the VSFs at all scales, but in particular the large scales, causing an elevation of ζ. However, the interaction between the clouds and the shocks lasts only for less than 0.6 Myr, after which ζ evolves back into the pre-shock conditions

The behaviour of M8 appears to contradict the **above explanations which we explain as follows**: In the beginning, M8 evolves only slightly. It loses a small fraction of gas (Paper II, Fig. 5, *middle* panel). Therefore, the VSFs increase towards larger separations. At $t = 1.5$ Myr the shock front of the $t = 0.8$ Myr SN hits the cloud. That causes a short period of extreme gravitational collapse, traced by the dip in ζ. As in the other clouds, the gas relaxes rapidly after the shock. However, the interaction with the shock the cloud has introduced instability into the clouds that continues to gravitationally contract. That is seen as slow decrease of ζ from $t = 1.8$ Myr on.

In summary, one can say that the scaling exponent, ζ, that is obtained by fitting a power-law relation onto the measured VSF, is a useful tool to understand and evaluate the time evolution of turbulence within molecular clouds. It is not only sensitive to both external (SNe) and internal (gravitational collapse) driving sources, but also reacts differently to the individual driving sources.

However, this diagnostic requires a series of time steps to be significant. According to She & Lévêque (1994) and Boldyrev (2002), $\zeta(3)$ is supposed to be equal or larger than unity whenever the gas experiences supersonic turbulence. Although this is definitely the case in the simulated clouds (Paper I; Paper II), one sees that $\zeta(3)$ declines far below 1 due to gravitational collapse. Thus, measuring ζ for individual moments in time, as observations would do, cannot fully describe the turbulence of molecular clouds.

The principle of "extended self-similarity" (Benzi et al. 1993, Sect. 2.2) offers a solution to this problem. The principle reflects the nature and the properties of intercloud turbulence, even when it is dominated by gravitational collapse. However, we also detect strong deviations that either reduce or increase the measured values of Z (see Fig. 3a). Those derivations can be related to the physical forces that currently dominate the clouds.

The peaks in the Z (for example, in M4 at $t = 4.1$ Myr) occur at the times when the respective $\zeta(3)$ reaches values close or below 0. This means that the VSF becomes flat ($\zeta = 0$) or increases forward smaller scales ($\zeta < 0$). In this case, self-gravitational contraction clearly dominates the cloud's evolution as it transfers turbulent power from the large to the small scales, where filaments and fragments are forming and accreting gas.

The decrease in Z (for example, in M3 around $t = 1.8$ Myr), on the other hand, occur when SN shocks hit and heavily impact the clouds. This causes a sudden, but heavy increase of turbulent power on all scales, though on the larger scales more than on the smaller, resulting in a steepening of the VSF towards larger scales and an increase in ζ. The VSFs become more sensitive to the shock the higher their order is. Therefore, the $\zeta(3)$ increases more rapidly than $\zeta(2)$ and $\zeta(1)$, causing $Z(2)$ and $Z(1)$ to decrease.

In summary, Z **is only a weak tracer for gravitational contraction, but a good tracer for shocks interacting with the cloud.** Whenever neither of these two extreme scenarios is acting on the clouds, the values of Z are close to the predicted values (see discussion below). This means that Z **and** ζ **are good tracers for processes suddenly driving turbulence within the cloud. However, when Z values are close to the ones predicted by theory, we cannot differentiate between freely decaying turbulence and moderate gravitational contraction**, as one can do it with ζ. However, the advantage is that a single-epoch observation of Z is sufficient to trace extreme motions and driving sources within observed molecular clouds.

Whenever the turbulence within the clouds is not driven in an extreme way one sees that the ratio of the VSF scaling exponents is mostly in agreement with predicted values for self-similar turbulence, although the clouds are dominated by gravitationally contracting motions during their evolution. **The measured values of** Z do not uniquely follow the predictions of only Boldyrev (2002) or She & Lévêque (1994), but are normally between the predicted values. Recalling that both studies describe supersonic, fully developed turbulent flows, the only difference between them is the geometry along which they allow the gas to flow. In the case of Boldyrev (2002), the gas flows are sheet-like, while they are filamentary in the work by She & Lévêque (1994).
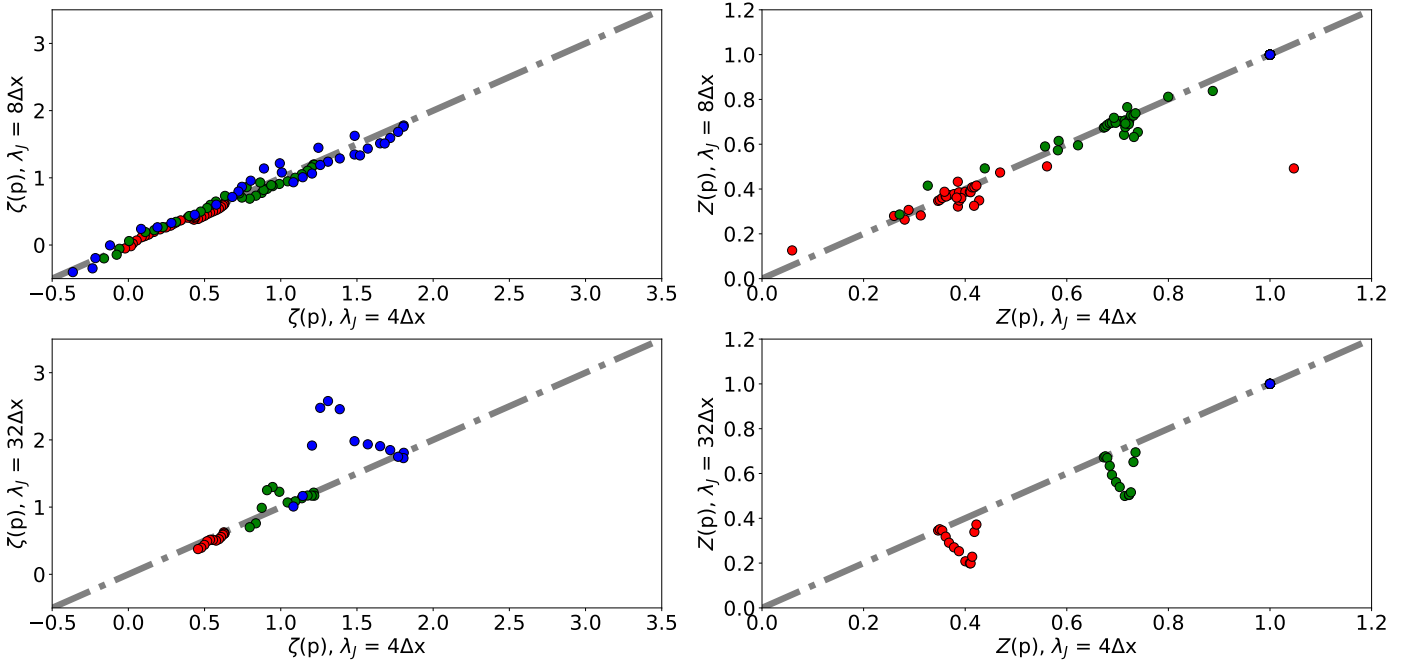
Figure 5: Comparison of measure VSF sclaing exponents, ζ (*left*), and self-similarity parameters, Z (*right*), depending on the Jeans refinement of the simulation runs the data are based on, respectively. The *abscissas*, thereby, always refers to the measurements based on $\lambda_J = 4\Delta x$, while the *ordinates* of the do so the $\lambda_J = 8\Delta x$ (*top*) and $\lambda_J = 32\Delta x$ (*bottom*) measurements. All data points based on the M3 cloud and represent the same time step in the respective simulations.

Since M3 is heavily impacted by many SN shocks and strong collapsing motions, it does not allow us to make strong predictions about its 'steady-state' evolution. The other two clouds, on the contrary, are less externally impacted. This allows us to relate the developments of measured Z to the internal evolution of the clouds. In M8, Z follows the predictions by She & Lévêque (1994) for most of the time. This **would suggest** that M8 mostly transfers gas along filamentary substructures which means that the cloud is highly hierarchically structured already at the beginning of the simulations and before self-gravity is active. This also implies that the formation of filamentary structures does not require gravity (e.g., Federrath 2016). The fact that we do not detect fragments before the clouds have evolved under the influence of self-gravity for at least one megayear (see Paper III), however, demonstrates that gravity is essential for the fragmentation of filaments and formation of further substructures.

The evolution of Z in M4 shows a slightly different picture. While the values of Z in M8 are mostly constant over time, they decrease in M4, starting at values that are in agreement with the sheet-like flows of Boldyrev (2002) to those that are predicted for filamentary flows by She & Lévêque (1994). This demonstrates that M4 develops its hierarchical structure as it evolves under the influence of self-gravity. As a consequence, its turbulent structure becomes more dominated by the filaments with time which causes the decline of Z. Considering that the gas of M4 is indeed first flattened into more sheet-like geometry through the impact of the SNe (Paper II) this observation is very interesting. It agrees with the studies, for example by Lin et al. (1965) or McKee & Ostriker (2007), that claim that molecular clouds are supposed to collapse in a dimension-losing, outside-in fashion that does not require any initial substructures within the clouds.

In summary, Z reflects the global geometry of turbulence within molecular clouds. Thereby, the measured values of Z are in good agreement with predictions from self-similarity theory,

as long as one carefully ensures that the dominating turbulence mode in the cloud matches the modes that are considered in the respective theory. This makes Z a reliable parameter for examining turbulence modes in observational studies. Furthermore, the time evolution of Z shows how the geometry of turbulence is changed due to the gravitational contraction, e.g. from sheet-like to filamentary vortices, accompanies the change of basic parameters describing the turbulent structure of the entire cloud. Z can also deviate from the predicted values. This, however, only occurs in time spans of extreme turbulence driving, such as SN shocks. Thereby, these extreme driving sources affect Z differently: SN shocks decrease Z, while gravity causes a **short-lived** peak in Z. In both cases, Z relaxes to the pre-perturbation values within a short time.

4.2. Comparison to Line-of-Sight Velocities

In this paper, we do not only aim to analyse the mechanisms that drive turbulence within simulated molecular clouds, but also to provide a practical tool that can be used to understand the dynamical processes within the ISM better. For the latter, it is necessary to examine its applicability under and the dependencies of the obtained results on all relevant conditions. As we have chosen to use VSFs for our analysis it is evident that we first need to investigate how the function reacts to the number of measured velocity vector components.

We recall that the VSF relates to the average relative velocity between the clouds' gas cells (see Eq. (1)). This means that for a proper analysis one needs all three components of the three-dimensional (3D) velocity vector for each contributing cell. Observations, however, normally measure only the one (1D) component along the line-of-sight (los), also known as local standard of rest velocity. If the gas moves exclusively along the los, both the 3D and 1D velocity measurements will return

the same VSF. If the gas is, contrary, moving along directions perpendicular to the los the 1D VSF will be absolutely 0.

In this section, we discuss the results considering this aspect. Hence, we use the same data of the model clouds as before and produce three subsamples by projecting the 3D velocity vectors onto the three major axes x, y, and z, respectively. The derived ζ and Z for each subsample are shown in Figs. 2b and 3b.

In Sect. 3.3 we have seen that the ζ and Z derived from the 1D VSFs generally evolve similarly as those derived from the 3D VSFs. Yet, we have also seen that individual sight lines may evolve differently. Those differences are generated when the gas is significantly more driven into the corresponding los than into the others (analogously to the simple scenario described above).

For example, for the first two megayears of the evolution of M4 the values of Z along the y axis are significantly higher than those observed along the other axes and the predicted values. Recalling that a higher value of Z correspond to an episode of very strong gravitational contraction, we can conclude that within this time span M4 is dominantly collapsing along its y axis. The values of Z that are measured for the other two axes agree with this conclusion as they are best predicted by Boldyrev (2002) who describes a sheet-like turbulence. Note that this effect is only visible as we analyse the three dimensions separately, while the driving of the gas along the y axis is averaged out in the 3D VSFs (see Fig. 3a).

In summary, we see that for a fully developed 3D turbulent field we expect that 1D VSFs behave similarly to 3D VSFs. However, when there is a preferred direction along which the gas flows the 1D and 3D VSFs differ significantly from each other. Thus, we predict that observed VSFs reflect the nature of turbulence within molecular clouds unless there is clear evidence that the gas is driven into a particular direction (e.g., by an proto-/stellar feedback, or SN shock front).

Note that in this analysis does not take typical los effects, such as optical depth effects or blending, into account. As we have seen in Sect. 3.4, a good knowledge of the origin of velocity information is essential for a proper interpretation of the obtained VSFs. Future studies need to investigate this point in more detail by performing elaborated radiative transfer calculations.

4.3. The Effect of Density Thresholds

In Sect. 3.4 we have tested the influence of the density threshold that defines the volume of interest on the behaviour of the VSF. In the work presented in this paper, we normally define the clouds as volumes of connected gas cells with number densities above $n_{cloud} = 100\ cm^{-3}$. Although this approach is in agreement with typical post-processing methods of observational data, it also means that we analyse only $\leq 1.5\%$ of the cubes' volumes, ignoring the more diffuse parts at the outer rims of the molecular clouds and the ISM. This raises the question: Are the turbulent motions within the entire ISM and the denser molecular clouds driven by the same processes? For targeting this question we have repleated our analysis and set $n_{cloud} = 0\ cm^{-3}$. Figs. 2c and 3c illustrate the results.

We see that the structure and behaviour of VSFs strongly depends on whether or not there is a density threshold. In the previous case, where $n_{cloud} = 100\ cm^{-3}$, we have seen a mostly straight decline of ζ and a rather constant evolution of Z over time that reflect the contraction of the clouds due to self-gravity.

Here, in the $n_{cloud} = 0\ cm^{-3}$ sample, we observe a completely different picture. There is still a slightly declining trend in ζ, yet

the evolutions are dominated by random fluctuations. We also see that the measured Z evolves completely constantly. This is true for the entire time range and the exactly same values of Z measured for all clouds. This can only be the case when the here analysed VSFs reflect the turbulent structure of the entire ISM in which all three clouds are embedded in. Furthermore, the source that drives the turbulence within the ISM acts constantly and isotropically on the diffuse gas. Thus, the ISM matter around the clouds can not be driven by individual events, like single SNe, as they do not have a high enough impact on the entire ISM, particularly not compared to the impact they have on individual molecular clouds that are comparably quiet zones within the ISM.

We conclude that the decision whether or not a density threshold is used for ascertaining insights on the turbulent composition of the observed gas has a significant and direct influence on the resulting VSFs. However, as mentioned previously, applying a density threshold is often unavoidable as it is a straightforward approach to filter the data on the actual area of interest. In observational studies it is even always present as minimal collision rates for excitation or the sensitivity of detectors automatically introduce an implicit density or intensity thresholds. Although we have only tested two specific setups in this context we have seen the significance of a proper choice of the density threshold, as well as a proper discussion of the obtained results considering the used threshold as one of the defining parameters.

4.4. The Effect of Density Weighting

In this subsection, we discuss the effect the ambiguous definition of VSFs has on the measurements. With this we mean that the VSF can be computed with or without taking density weighting into account. This ambiguity originates in the type of data one analyses. In general, the VSF considers the average relative velocity between two individual Lagrangian particles or turbulent vortices. As each particle stores its complete set of information, its mass, and therefore its inertia, is automatically considered when iterating its velocity. This makes Eq. (6) sufficient for deriving the VSF of the fluid properly.

In our case, however, we examine Eulerian data that store the parameters of the fluid on a static grid. The information of individual particles and vortices are, thereby, averaged over the grid. Consequently, it is important to consider this when computing the VSF. This is done by using the density-weighted definition of the VSF given in Eq. (1).

Although the motivation why there are different definitions of the VSF and why they are used for non-overlapping samples of data, it is not yet clear how the results obtained with the two approaches relate to each other. We investigate that question by applying both approaches on our data. The results are presented in Sect. 3.5.

We see that, as long as the turbulence is dominated by the large scales, considering the density weighting or not does not have a significant effect on the data. However, as the clouds evolve the differences increase because the non-weighted VSFs never drop below 0.5. This is because the non-weighted VSF treats all cells equally, no matter whether the particular cell represents a dense element of the cloud centre or a diffuse element of the cloud's edge, while the weighted VSF gives more weight to the matter within the clouds. As long as the turbulence is dominated by large scales this does not cause a notable difference as these long separations represent cells on the outer surface of the clouds, with similar densities and conditions. The small lag scales, contrary, reflect how the conditions change within the

clouds, with density gradients becoming larger towards the centre of the clouds and increasing faster than the relative velocities of neighbouring cells. In this case, the density weighting becomes crucial to compensate for the fact that the higher density represents a higher number of particles in a Lagrangian framework. However, if one does not consider this (as we do when using the non-weighted definition of the VSF) the inner regions of the clouds are not processed correctly. This ends in a situation where the large scales never seem to loose their dominance in term of kinetic energy, and ζ never becomes close or less than 0; a situation that does not reflect the reality.

In summary, we can trace the discrepancies between the scaling exponents of density-weighted and non-weighted VSFs back to the **inability** of the non-weighted VSFs to follow the transition form large-scale driven to small-scale dominated distributions of turbulent power.

Nevertheless, Fig. 3d illustrates that these differences can be traced by ζ only. Besides the features created when ζ becomes close to 0 in the density-weighted VSFs, the measured Z have similar values, evolve and reacts to external driving mechanisms similarly independently based on which approach they are computed. This observation is true for all Jeans refinement levels, as Fig. 4 demonstrates.

We conclude that deriving the VSF from smooth density distributions without considering density weighting does not affect the behaviour of ζ and Z, as long as the turbulence is dominated by large scale vortices, while it has a significant effect on the measurements when the small scales become dominant. The latter is particularly important as this finding has a directly impact on the conclusions drawn based on the scales and mechanisms that drive the turbulence based on the measured ζ. Not only does ζ become insensitive from the influence of gravitational contraction with time, the non-weighted VSFs do also not reflect when the majority of kinetic energy has been transferred to small scales. Thus, it is highly important to clarify which definition of VSF is used and if it is indeed suitable for the respective study. Yet, our analysis also shows that the principle of self-similarity relativises the deviations between the two approaches as the different orders of the VSFs keep scaling in the same way relative to each other.

4.5. The Effect of Jeans Length Refinement

In Sect. 3.6, we have motivated the need to investigate the influence of Jeans refinement on VSFs. In particular, we examine how the choice of using the minimal required refinement compares to a generally recommended refinement level, including the differences in total energy and resonances seen in the power spectra. To do this, we use the data by Paper II that resolve the Jeans length in M3 twice ($\lambda_J = 8\Delta x$) and eight times ($\lambda_J = 32\Delta x$) finer as the original simulations ($\lambda_J = 4\Delta x$).

In Fig. 5 we see that the choice of refinement level does not have to have a significant influence on the measurements and evolution of both ζ and Z. $\lambda_J = 4\Delta x$ and $\lambda_J = 8\Delta x$ are in very good agreement with each other. This means that, although refining Jeans lengths with 4 cells misses about 13% of kinetic energy, the effect on the structure and behaviour of the turbulence is rather small and not traced by the VSF analysis.

However, Fig. 5 shows that such an agreement is not given with $\lambda_J = 32\Delta x$, as latter differs more from $\lambda_J = 4\Delta x$ the higher the order of the VSF is. Following the explanations in Sect. 3.6, the behaviour of ζ and Z in the $\lambda_J = 32\Delta x$ runs corresponds to the reaction of the cloud's gas to a shock wave running through the cloud; caused by a supernova that exploded before $t = 0$ Myr.

Indeed one sees a SN at a distance of 172 pc at $t = -1.11$ Myr. Due to the distance the SN is too weak to effectively compress the gas within M3 and causing a shock. This is why it has not been detected previously in the less refined samples. However, the SN explodes far below the mid-plane of the simulated disk galaxy, in a region without dense gas. This means that the shock wave, that has been injected by the explosion, is less damped as it propagates through the ISM. By the time the front arrives at M3 it is still energetic enough to drive strong winds, with velocities above 300 km s^{-1}, at the closer edge of the cloud. This causes an increase of VSFs at longer lag scales and the increase of ζ, as well as the drop in Z.

Derivations of measured Z to predicted values do trace external turbulent driving. Whether the source is a SN shock front propagating through the cloud or a strong wind, cannot be distinguished by Z only. Yet, Z remains a fine probe for the geometry of turbulence and the scales at which turbulence is driven.

4.6. Comparison to Observational Data

[completely new]

5. Summary & Conclusions

In this paper, we analyse the turbulent structures of molecular clouds that have formed within three-dimensional adaptive mesh FLASH simulations of the self-gravitating, magnetised, SN-driven ISM by Ibáñez-Mejía et al. (2016). The main results are as follows.

– The scaling of velocity structure functions (VSFs) is sensitive to both internal (gravitational contraction) and external (SN shocks, winds) driving sources of turbulence. Applied on simulated data, the time evolution of the scaling exponent, ζ, can reveal which driving mechanism dominates the turbulence of an entire molecular cloud. The self-similarity parameter, Z, though, is not directly sensitive to gravitational contraction. Yet, it can be used as observational tracer **for recent interactions with** SNe and winds.

– As long as the molecular cloud is not affected by a shock, Z is in good agreement with predicted values for supersonic flows. This makes it a fine probe for the properties of dominant turbulent modes, such as the geometry, and their evolution in the context with the evolution of the cloud.

– We test the influence of Jeans refinement on the VSFs. We find that the absolute amount of kinetic energy does not influence the evolution of ζ and Z, as long as the power spectrum is properly resembled, or similarly resembled by the compared samples.

– We see that the behaviour of the VSFs can be tracked with similar results based on 3D (i.e., from simulated data) and 1D (i.e., from observational data) velocity information, as long as there is no dominating flow driving the gas into a direction perpendicular to the line of sight. In the general case of a fully developed turbulent field, both ζ and Z evolve similarly in both scenarios, even though the actual values might not be in good agreement.

– We test the influence of introducing a density threshold on the VSFs. We see both quantitative and qualitative differences. The VSFs that based on the unfiltered data are much steeper than the cloud-only VSFs and do not reflect any interaction with any of the driving sources, including SN shocks. The measured Z values are constant in time and and for all clouds. This means that the turbulence we examine in this

| Reference	Target Object(s)	p	ζ	Z
Heyer & Brunt (2007)	^{12}CO J = 1-0	1	0.49 ± 0.15	0.49 ± 0.15
Heyer & Dame (2015)	30 MCs	1	0.24 ± 0.00	0.24 ± 0.00
	Taurus	1	0.26 ± 0.00	0.26 ± 0.00
Miesch & Bally (1994)	^{13}CO J = 1-0	1	0.43 ± 0.15	0.43 ± 0.15
		2	0.86 ± 0.30	0.86 ± 0.30
Padoan et al. (2003)	Perseus	1	0.50 ± 0.00	0.42 ± 0.00
		2	0.83 ± 0.00	0.72 ± 0.00
		3	1.18 ± 0.00	1.00 ± 0.00
	Taurus	1	0.46 ± 0.00	0.42 ± 0.00
		2	0.77 ± 0.00	0.72 ± 0.00
		3	1.10 ± 0.00	1.00 ± 0.00
Padoan et al. (2006)	Perseus	2	0.80 ± 0.10	0.80 ± 0.10
Roman-Duval et al. (2011)	^{13}CO J = 1-0	1	0.50 ± 0.30	0.50 ± 0.30
Zernickel (2015)	NGC 6334	1	0.38 ± 0.00	0.38 ± 0.00
		2	0.76 ± 0.01	0.76 ± 0.01
	NGC 6334	1	0.48 ± 0.01	0.48 ± 0.01
	($\ell \leq 4$ pc)	2	0.79 ± 0.01	0.79 ± 0.01

Table 1: Summary of observed ζ and Z in the literature.
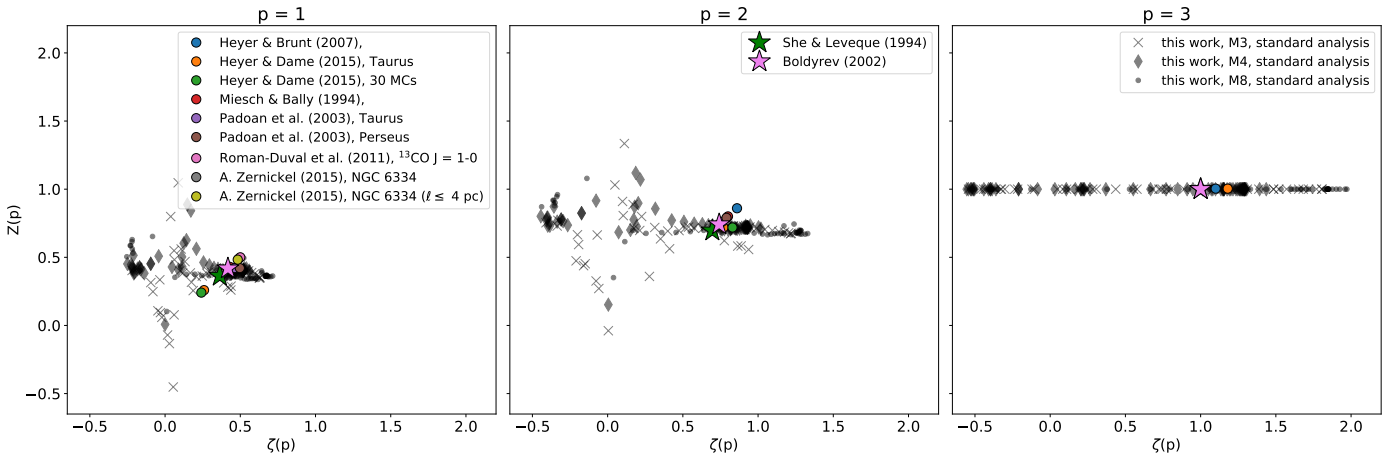
Figure 6: Summary of measurements of ζ (*abscissas*) and Z (*ordinates*) for orders $p = 1$–3 (from *left* to *right*) in this study and in the literature. The grey markers represent the values as presented in Sect. 3.2, while the coloured star markers illustrate the predictions by She & Lévêque (1994) and Boldyrev (2002). The coloured, circular marker summarise values found in the literature (see legend for precise references).

sub-project reflects the ISM in our entire galactic-scale simulations. The values of Z are slightly below the value predicted for a filamentary flow by She & Lévêque (1994). We conclude that the turbulence in the modelled ISM consists of vortices that are similar to filamentary flows, yet with a ratio of average length scale of the two moments being more equal to unity than in the filamentary case.

– We investigate the influence of defining the VSF with and without taking density weighting into account. We see that the qualitative behaviour is traced by both approaches. Yet, the scaling of the non-weighted VSF is always positive and evolve flatter than they do for the density-weighted VSF. This means that non-weighted VSFs that are based on smoothed density distributions are biased against large scale motions and may not reveal the entire distribution of turbulent power within a molecular cloud.

Our analysis shows that VSFs are fine tools for examining the driving source of turbulence within molecular clouds. Therefore, we recommend its usage in future studies of molecular clouds. However, studies that utilise VSFs need to precisely review the assumptions and parameters they imply in their anal-

ysis as those can have a significant influence on the out-coming results.

For the simulated clouds, the VSFs illustrate that gravitational contraction dominates the evolution of the clouds, with short periods within which SN shock waves accelerate the turbulent powers on all scales. However, it requires further studies to verify this to be the common fragment formation scenario. In particular, a higher Jeans length refinement is needed to resolve the velocity structures on scales of individual grid cells (0.1 pc in this case) better. This is crucial for following the local behaviour of the gas as neither the average behaviour of the filaments nor the dominant turbulence driving source of the entire molecular clouds mirror the underling flow patterns of the gas that is related to fragmentation and the formation of future star formation activity.

References

Ballesteros-Paredes, J., Hartmann, L. W., Vázquez-Semadeni, E., Heitsch, F., & Zamora-Avilés, M. A. 2011a, Monthly Notices Roy. Astron. Soc. , 411, 65

Ballesteros-Paredes, J., Vázquez-Semadeni, E., Gazol, A., et al. 2011b, Monthly Notices Roy. Astron. Soc. , 416, 1436

Banerjee, S. & Galtier, S. 2013, Phys. Rev. E., 87, 013019

Benzi, R., Biferale, L., Fisher, R., Lamb, D. Q., & Toschi, F. 2010, Journal of Fluid Mechanics, 653, 221

Benzi, R., Ciliberto, S., Tripiccione, R., et al. 1993, PhysRevE, 48, R29

Boldyrev, S. 2002, Astrophys. J. , 569, 841

Boneberg, D. M., Dale, J. E., Girichidis, P., & Ercolano, B. 2015, Monthly Notices Roy. Astron. Soc. , 447, 1341

Brunt, C. M. & Heyer, M. H. 2013, Monthly Notices Roy. Astron. Soc. , 433, 117

Brunt, C. M., Heyer, M. H., & Mac Low, M.-M. 2009, Astron. Astrophys. , 504, 883

Burkhart, B., Collins, D. C., & Lazarian, A. 2015, Astrophys. J. , 808, 48

Chira, R.-A., Kainulainen, J., Ibáñez-Mejía, J. C., Henning, T., & Mac Low, M.-M. 2018, Astron. Astrophys. , 610, A62

Dekel, A. & Krumholz, M. R. 2013, Monthly Notices Roy. Astron. Soc. , 432, 455

Federrath, C. 2016, Monthly Notices Roy. Astron. Soc. , 457, 375

Fleck, Jr., R. C. 1980, Astrophys. J. , 242, 1019

Fryxell, B., Olson, K., Ricker, P., et al. 2000, Astrophys. J. Suppl., 131, 273

Galtier, S. & Banerjee, S. 2011, Physical Review Letters, 107, 134501

Gotoh, T., Fukayama, D., & Nakano, T. 2002, Physics of Fluids, 14, 1065

Hartmann, L., Ballesteros-Paredes, J., & Heitsch, F. 2012, Monthly Notices Roy. Astron. Soc. , 420, 1457

Heyer, M. & Dame, T. M. 2015, Ann. Rev. Astron. Astrophys. , 53, 583

Heyer, M. H. & Brunt, C. 2007, in IAU Symposium, Vol. 237, Triggered Star Formation in a Turbulent ISM, ed. B. G. Elmegreen & J. Palous, 9–16

Heyer, M. H. & Brunt, C. M. 2004, Astrophys. J. Lett. , 615, L45

Ibáñez-Mejía, J. C., Mac Low, M.-M., Klessen, R. S., & Baczynski, C. 2016, Astrophys. J. , 824, 41

Ibáñez-Mejía, J. C., Mac Low, M.-M., Klessen, R. S., & Baczynski, C. 2017, Astrophys. J. , 850, 62

Kolmogorov, A. 1941, Akademiia Nauk SSSR Doklady, 30, 301

Krumholz, M. R., Bate, M. R., Arce, H. G., et al. 2014, Protostars and Planets VI, 243

Lin, C. C., Mestel, L., & Shu, F. H. 1965, Astrophys. J. , 142, 1431

Mac Low, M.-M. 2003, in Lecture Notes in Physics, Berlin Springer Verlag, Vol. 614, Turbulence and Magnetic Fields in Astrophysics, ed. E. Falgarone & T. Passot, 182–212

Mac Low, M.-M. & Klessen, R. S. 2004, Reviews of Modern Physics, 76, 125

McKee, C. F. & Ostriker, E. C. 2007, Ann. Rev. Astron. Astrophys. , 45, 565

McKee, C. F. & Zweibel, E. G. 1992, Astrophys. J. , 399, 551

Miesch, M. S. & Bally, J. 1994, Astrophys. J. , 429, 645

Miyamoto, Y., Nakai, N., & Kuno, N. 2014, PASJ, 66, 36

Padoan, P., Boldyrev, S., Langer, W., & Nordlund, Å. 2003, Astrophys. J. , 583, 308

Padoan, P., Juvela, M., Kritsuk, A., & Norman, M. L. 2006, Astrophys. J. Lett. , 653, L125

Padoan, P., Pan, L., Haugbølle, T., & Nordlund, Å. 2016, Astrophys. J. , 822, 11

Roman-Duval, J., Federrath, C., Brunt, C., et al. 2011, Astrophys. J. , 740, 120

Schmidt, W., Federrath, C., & Klessen, R. 2008, Physical Review Letters, 101, 194505

Seifried, D., Walch, S., Girichidis, P., et al. 2017, ArXiv e-prints

She, Z.-S. & Lévêque, E. 1994, Physical Review Letters, 72, 336

Tan, J. C., Shaske, S. N., & Van Loo, S. 2013, in IAU Symposium, Vol. 292, Molecular Gas, Dust, and Star Formation in Galaxies, ed. T. Wong & J. Ott, 19–28

Truelove, J. K., Klein, R. I., McKee, C. F., et al. 1998, Astrophys. J. , 495, 821

Turk, M. J., Oishi, J. S., Abel, T., & Bryan, G. L. 2012, Astrophys. J. , 745, 154

Zernickel, A. 2015, PhD thesis, I. Physikalisches Institut der Universität zu Köln, Zülpicher Straße 77, 50937, Köln, Germany ¡EMAIL¿zernickel@ph1.uni-koeln.de¡/EMAIL¿